KeA1

CHINESE ROOTS
GLOBAL IMPACT

Contents lists available at ScienceDirect

Petroleum Science

journal homepage: www.keaipublishing.com/en/journals/petroleum-science



Original Paper

Fractures interaction and propagation mechanism of multi-cluster fracturing on laminated shale oil reservoir



lia-Xin Lv b, c, Bing Hou a, b, c, *

- a Department of Petroleum Engineering, China University of Petroleum (Beijing) at Karamay, Karamay, 834000, Xinjiang, China
- b Key Laboratory of Petroleum Engineering, Ministry of Education, China University of Petroleum (Beijing), Beijing, 102249, China
- ^c State Key Laboratory of Petroleum Resources and Engineering, China University of Petroleum (Beijing), Beijing, 102249, China

ARTICLE INFO

Article history: Received 12 July 2023 Received in revised form 27 November 2023 Accepted 4 February 2024 Available online 10 February 2024

Edited by Meng-Jiao Zhou

Keywords: Laminated shale Multi-cluster fracturing Cross-layer Cohesive zone model Acoustic emission technique

ABSTRACT

The continental shale reservoirs of Jurassic Lianggaoshan Formation in Sichuan Basin contain thin lamina, which is characterized by strong plasticity and developed longitudinal shell limestone interlayer. To improve the production efficiency of reservoirs by multi-cluster fracturing, it is necessary to consider the unbalanced propagation of hydraulic fractures and the penetration effect of fractures. This paper constructed a numerical model of multi-fracture propagation and penetration based on the finite element coupling cohesive zone method; considering the construction cluster spacing, pump rate, lamina strength and other parameters studied the influencing factors of multi-cluster fracture interaction propagation; combined with AE energy data and fracture mode reconstruction method, quantitatively characterized the comprehensive impact of the strength of thin interlayer rock interfaces on the initiation and propagation of fractures that penetrate layers, and accurately predicted the propagation pattern of hydraulic fractures through laminated shale oil reservoirs. Simulation results revealed that in the process of multi-cluster fracturing, the proportion of shear damage is low, and mainly occurs in bedding fractures activated by outer fractures. Reducing the cluster spacing enhances the fracture system's penetration ability, though it lowers the activation efficiency of lamina. The high plasticity of the limestone interlayer may impact the vertical propagation distance of the main fracture. Improving the interface strength is beneficial to the reconstruction of the fracture height, but the interface communication effect is limited. Reasonable selection of layers with moderate lamina strength for fracturing stimulation, increasing the pump rate during fracturing and setting the cluster spacing reasonably are beneficial to improve the effect of reservoir stimulation.

© 2024 The Authors. Publishing services by Elsevier B.V. on behalf of KeAi Communications Co. Ltd. This is an open access article under the CC BY-NC-ND license (http://creativecommons.org/licenses/by-nc-nd/

4.0/).

1. Introduction

The Jurassic system in the Sichuan Basin is rich in tight oil and shale gas, among which the onshore shale gas resources are rich in reserves and have broad development prospects (Zhang et al., 2022; Yang et al., 2022). Horizontal well with multi-stage/multicluster fracturing technology can shorten the distance of fluid percolation into the fracture, increase the volume of drainage, and improve oil and gas production, and has become an effective technology for shale reservoir development (Cheng, 2012; Dontsov and Suarez-Rivera, 2020). In the Bakken and EagleFord marine

shale gas blocks in North America, horizontal wells and multicluster fracturing were used to achieve beneficial development of shale reservoirs under certain well spacing conditions (Singh et al., 2019). In the southern Sichuan Basin shale gas block, a field trial of multi-cluster fracturing was conducted to increase the number of clusters and shorten the cluster spacing to improve the fracture complexity (Jin et al., 2021). Based on field experience and previous studies, it was found that the cluster spacing requirement for horizontal wells is strict for the multi-cluster process, reducing the cluster spacing will lead to serious stress interference and competitive propagation between fractures, while increasing the cluster spacing will make the formation of complex fracture networks more difficult (Hossain and Rahman, 2008). Lu and He (2022) studied the initiation and propagation of perforation fractures. It is found that the initial initiation rate and the length of the

^{*} Corresponding author. Department of Petroleum Engineering, China University of Petroleum (Beijing) at Karamay, Karamay, 834000, Xinjiang, China. E-mail address: binghou@cup.edu.cn (B. Hou).

hydraulic fracture, and the generated fracture number, can be used as indicators of fracture competition. Perforated fractures will eventually form a fracture propagation mode dominated by several main fractures and supplemented by microfractures. It is important to reasonably optimize the number of injection clusters, construction parameters and related supporting technologies (Li and Wu, 2022a) to form an in-segment multicluster fracturing technique suitable for the geological and engineering characteristics of the study area (Hou et al., 2019; Zhang et al., 2021).

Based on the above engineering background, experimental and numerical simulation methods to study the mechanical mechanism of unbalanced multifracture propagation have been proposed one after another, and due to the limitations of physical modeling in experiments, numerical simulation has been widely used to analyze the fracture initiation and propagation behavior of multi fractures (Chen et al., 2018; Wang et al., 2021). Currently, many numerical methods have been developed to simulate the propagation behavior of multi fractures during cross-layer fracturing, including the finite element method (Zhu, et al., 2015; Han et al., 2020), discrete element method (Chang and Hou, 2022), and displacement discontinuity method (Li et al., 2021; Li et al., 2022), which are used more frequently. Lecampion (2009) used a special fracture tip enhancement function in their study to represent the unique tip multiscale asymptotic relationship of hydraulic fractures, which enabled the XFEM (extended finite element method) to achieve better simulation results for hydraulic fracture propagation problems.

Wu et al. (2017) investigated the impact of irregular fracture spacing on non-uniform fracture growth. It was shown that for simultaneous multiple fracture propagation, non-uniform flow rate distribution is induced because stress shadow effects exert additional flow resistance on the interior fractures. Decreasing perforation diameter or the number of exterior fractures can promote even fracture growth. Liu et al. (2020) used lattice simulation method to investigate multi-cluster hydraulic fracturing. The results showed that cluster spacing plays an important role in geometry of the propagating fracture. The center hydraulic fracture is restricted to propagate when cluster spacing is decreased. Chen et al. (2020) proposed an algorithm for a planar 3D multi-fracture model for horizontal well-staged fracturing. The results showed that the heterogeneity of in-situ stress among multiple clusters has a more significant effect on fluid distribution than stress interference when the perforation number is the same in each cluster. They proposed that increasing the number of perforations in the highstress zone can uniform fluid distribution. Previous studies have shown that the fracturing effect is also affected by the development of lamina in shale, and the weak cementation of lamina leads to typical heterogeneity in deformation characteristics, tensile strength, and fracture toughness of shale (Jin et al., 2021). Hou et al. (2022) used a 3D lattice algorithm hydraulic fracturing simulator to study the effects of perforation position and length on hydraulic fracture propagation. Achieving maximum stimulated volume requires consideration of lithologic sequence, coal seam thickness, stress states, and rock properties. To improve the combined gas production in coal measure strata, it is possible to simultaneously stimulate multiple coal seams or adjacent gas-bearing sandstones.

Jurassic Lianggaoshan Formation in Fuxing area of Sichuan Basin developed dark muddy shale interbedded with thin lamina, which has great primary quality of shale oil and favorable conditions for shale reservoir development. At present, there are few researches on numerical simulation of horizontal well multi-cluster and cross-layer fracturing. This paper establishes a multi-fracture hydraulic fracturing model based on cohesive element method containing lamina structure, uses python to write a program to extract

information of fracture parameters, analyzes AE events during fracturing to study the effects of different geological and engineering parameters on fracture propagation and morphology, and reveals the influence of lamina strength on fracture. The effect of different geological and engineering parameters on fracture propagation and fracture morphology was investigated.

2. Horizontal well multi-cluster cross-layer fracturing model

2.1. Engineering and geological background

The terrestrial shale in the Lianggaoshan Formation of the Fuxing area is of good primary quality and has the material basis for the formation of large oil and gas reservoirs (Fig. 1). The area is characterized by low hills and hilly terrain, and the Lianggaoshan Formation is buried at moderate depths, with less faults, and is dominated by black and gray mudstones, interbedded with shell limestone interlayers and thin silt layers.

Well T takes the shale gas interval in the second member of Lianggaoshan Formation of Middle Jurassic System as the target stratum. The completed drilling depth is 2639 m, and the horizontal section is 1502 m. The completed drilling horizon is Daanzhai section of Ziliujing Formation of Lower Jurassic System. The shale gas reservoir of Jurassic Lianggaoshan Formation is located in the arc-shaped high-steep fold belt in Sichuan Basin, and is mainly composed of abnormally low-pressure tight sandstone oil and gas reservoirs and normal-pressure condensate gas reservoirs.

The Lianggaoshan Formation is subdivided into 8 sublayers according to the characteristics of lithological combination and electric survey curve (Fig. 2): Layer 7 is primarily composed of mudstone. Layer 6 is primarily composed of sandy mudstone. Layer 5 is primarily composed of mud shale. Layer 3 is primarily composed of shale, and a 0.28 cm-thick shell limestone develops in the middle and upper part. Layers 2, 4, and 6 are primarily composed of sandstone with high density, low sound wave, relatively compact rock, and lower porosity and permeability than shale and conventional sandstone.

Well T targets the shale gas formation in the second member of the Middle Jurassic Lianggaoshan Formation. The well started sidetracking at 2150 m and landed at the target point at the depth of 2825 m, and the drilling was completed in layer 4 of the second member of Lianggaoshan Formation. The drilled formations include lower Shaximiao Formation of the Middle Jurassic System, the third member of Lianggaoshan Formation, and the second member of the Lianggaoshan Formation. Each fracturing section in the well is divided into 3–10 clusters of perforations to complete the well. The geological structure of layers 1–7 is relatively complex, and their lithological combinations are representative in the Ziliujing Formation reservoir. It is an ideal choice to study the influence of T well on multi-fracture propagation under different factors such as cluster spacing, pump rate, and interface strength.

2.2. Principle of numerical calculation

The CZM (cohesive zone model) based on FEM (finite element method) of viscoelastic-plastic damage model introduces a cohesive element layer with material strength at the mesh boundary of the continuous medium, and simulates the propagation behavior of fractures within the medium through the fracture of the cohesive element layer, which can effectively avoid the generation of fracture tip singular behavior in the fracture process and mesh division and other problems. Fig. 3 shows a schematic diagram of the two-dimensional cohesive element geometry. The blue nodes around the cohesive element are cohesive viscoelastic nodes, which do not

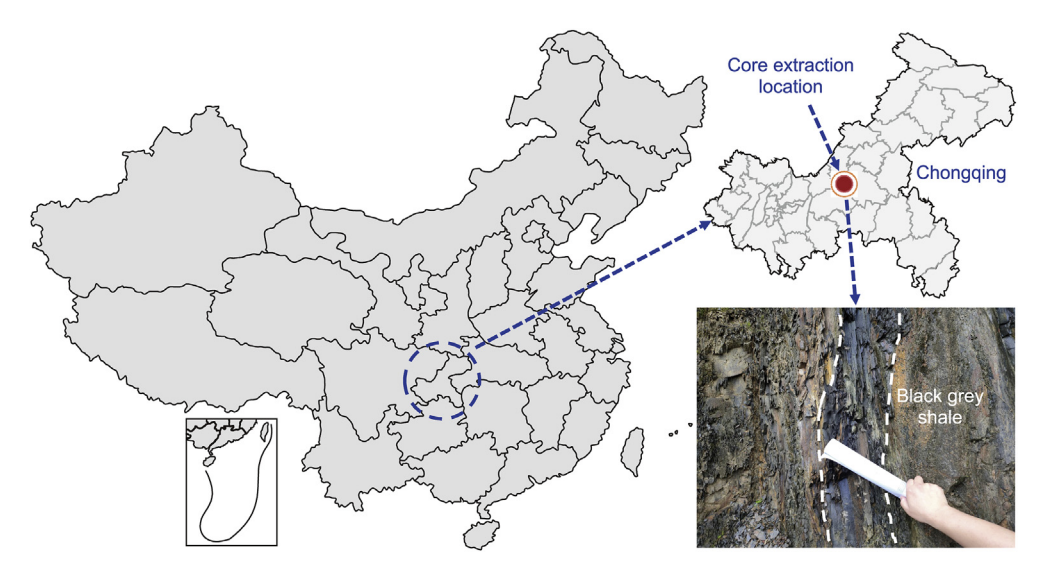


Fig. 1. Downhole cores of continental shale reservoir in Lianggaoshan section.

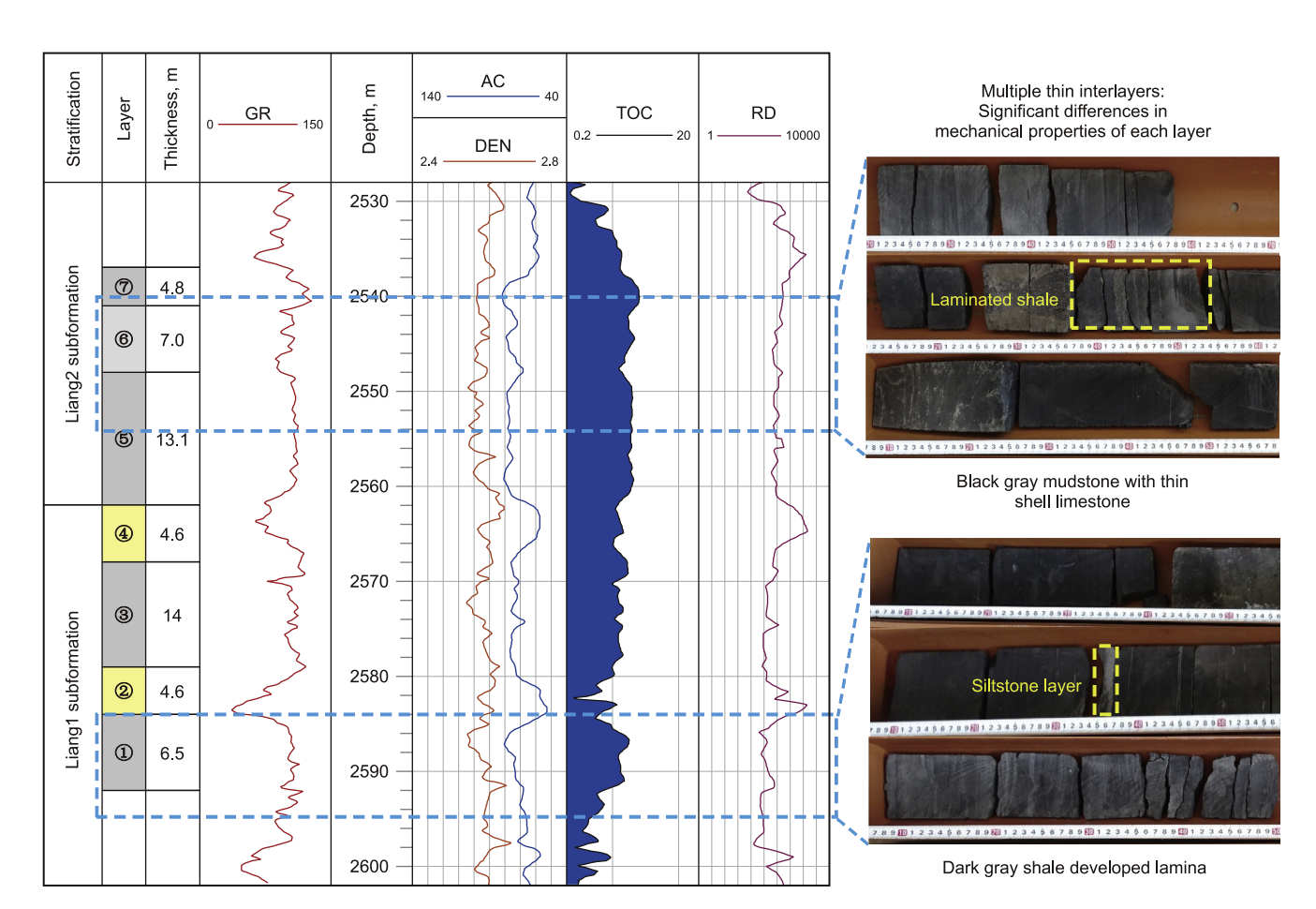


Fig. 2. Comprehensive stratigraphic column of Well T and distribution characteristics of core.

have pore pressure degrees of freedom; the nodes in the middle layer are pore pressure nodes, creating a potential path for the propagating hydraulic fracture.

The following stress-strain relationship needs to be satisfied before damage starts to occur in the cohesive elements (Diehl, 2008), and the expression of the traction stress vector t to which the cell is subjected is shown below:

where K, σ , and ε are the elastic modulus, nominal traction vector, and strain, respectively; the subscripts n, s, and t are the normal

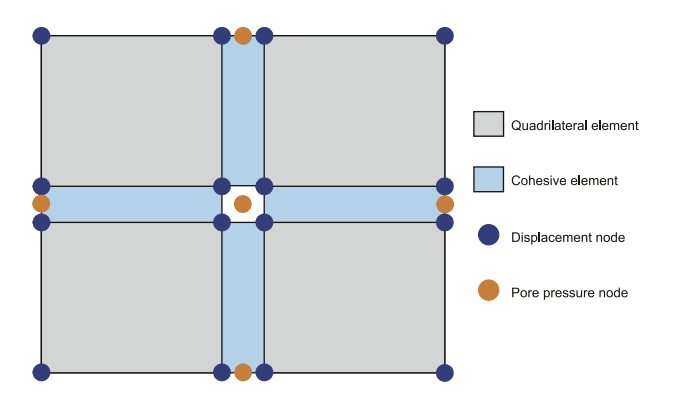


Fig. 3. Schematic diagram of a cohesive element embedded between quadrilateral elements.

direction and two local shear directions, respectively.

$$\int_{V} (\overline{\sigma} - \mathbf{I} p_{\mathbf{W}}) \delta \varepsilon dV = \int_{S} t \cdot \delta v dS + \int_{V} f \cdot \delta v dV$$
 (2)

where $\overline{\sigma}$ is the effective stress, Pa; **I** is unit matrix; p_w is pore pressure, Pa; $\delta \varepsilon$ is the virtual rate of deformation, s^{-1} ; t is the surface traction per unit area, N/m^2 ; f is the body force per unit volume, N/m^3 ; dS is the load action area, m^2 ; dV is the element volume, m^3 .

In numerical calculations, adding pore pressure degrees of freedom to the divided grid nodes, that is, attaching pore pressure to each node, can simulate the flow of fluid in reservoir pores. Based on the principle of fluid mass conservation, which means that the total mass of fluid flowing into the reservoir matrix within a certain period is equal to the sum of the increase in fluid volume in the reservoir matrix and the mass of fluid flowing out, the mass conservation equation for fluid flow in rock pores is derived. The equivalent integral weak form expression is

$$\int_{V} \frac{1}{I} \frac{\mathrm{d}}{\mathrm{d}t} (J \rho_{w} n_{w}) \mathrm{d}V + \int_{S} \rho_{w} n_{w} \boldsymbol{n} \cdot v_{w} \mathrm{d}S = 0$$
(3)

where J is the change rate of reservoir pore volume; $n_{\rm w}$ is the ratio of liquid volume in pores to total reservoir volume; $\rho_{\rm w}$ is pore liquid density, kg/m; \boldsymbol{n} is the outer normal vector of surface S; $\nu_{\rm w}$ is average velocity of fluid in pores, m/s.

Assuming that the basic behavior of pore fluid flow in the reservoir matrix follows Darcy's law, which is generally used to describe low-speed fluid flow and conforms to the percolation law of fluid in the matrix during hydraulic fracturing. Flow velocity expression

$$\mathbf{v}_{\mathsf{W}} = -\frac{1}{\phi g \rho_{\mathsf{W}}} \mathbf{K} \left(\frac{\partial p_{\mathsf{W}}}{\partial x} - \rho_{\mathsf{W}} g \right) \tag{4}$$

where g is the gravitational acceleration, kg/s^2 ; ϕ is porosity; $\textbf{\textit{K}}$ is the permeability coefficient tensor.

Characterizing Darcy's law with permeability coefficient K, the dimension is velocity, while permeability k is a parameter that reflects the structural characteristics of porous media in a reservoir, and the dimension is area. The conversion relationship between them is

$$k = \frac{K\rho_{\rm W}g}{\mu} \tag{5}$$

In this study, the fracture initiation process satisfies the maximum nominal stress criterion (Wang, et al., 2020). The calculation equation for the maximum nominal stress criterion is as follows:

$$\max\left\{\frac{\langle \sigma_{n} \rangle}{T}, \frac{\sigma_{s}}{\sigma_{s}^{0}}, \frac{\sigma_{t}}{\sigma_{t}^{0}}\right\} = 1$$
 (6)

where superscript 0 represents the peak stress value in the three directions. The fracture begins to form when the maximum nominal stress ratio reaches 1. When the cohesive element is under pressure or compressive deformation does not appear to be damaged, it can be expressed by the following equations:

$$\langle \sigma_n \rangle = \begin{cases} \sigma_n & \sigma_n \ge 0 \\ 0 & \sigma_n < 0 \end{cases} \tag{7}$$

During the damage process, the elastic modulus declines, according to the linear degradation criterion.

$$E = (1 - D) \times E^0 \tag{8}$$

where E^0 and E represent the modulus of elasticity before and after the damage to the element, respectively.

The rock stiffness degradation and structural failure will happen if the traction force meets the initial damage criterion (Eq. (6)). In this study, the mechanical behavior following damage initiation was described using linear softening. Eq. (9) can be used to express the traction-separation constitutive relation of the bilinear cohesive element (Liu, et al., 2018). The damage factor (*D*), ranging from 0 to 1, was developed to characterize the degree of rock damage.

$$T = \begin{cases} K_0 d_{\rm m} & 0 < d_{\rm m} \le d_{\rm m}^0 \\ (1 - D) K_0 d_{\rm m} & d_{\rm m}^0 < d_{\rm m} < d_{\rm m}^f \\ 0 & d_{\rm m} \ge d_{\rm m}^f \end{cases}$$
(9)

The scalar damage variable D is used to express the degree of damage and the calculation equation is as follows:

$$D = \frac{d_{\rm m}^{\rm f} \left(d_{\rm m}^{\rm max} - d_{\rm m}^{\rm 0}\right)}{d_{\rm m}^{\rm max} \left(d_{\rm m}^{\rm f} - d_{\rm m}^{\rm 0}\right)} \tag{10}$$

The overall degree of material damage, denoted as D, is defined by Eq. (10) (Zhang et al., 2010). In this equation, T represents the traction force, $d_{\rm m}$ is the relative displacement between the top and bottom surfaces of cohesive elements, K_0 is the initial stiffness of cohesive elements, $d_{\rm m}^{\rm m}$ is the displacement at the initial failure of the element, $d_{\rm m}^{\rm f}$ is the displacement at material failure (D=1), and $d_{\rm m}^{\rm max}$ is the maximum displacement during loading. When the displacement of cohesive elements is below the damage threshold ($d_{\rm m}^{\rm 0}$), the material is in an elastic state (D=0). With the increasing displacement, damage occurs to the rock. The material's stiffness degenerates to $(1-D)K_0$. Ultimately, the separation displacement reaches the failure threshold, and the material is considered completely damaged (T=0 and D=1).

To reflect the influence of shale lamina structure on fracture propagation, the lamina strength index was defined based on the rock mechanical properties of the target reservoir.

$$\gamma_{\rm l} = \frac{T_{\rm l}/T_{\rm r}}{2} \tag{11}$$

where γ_1 is the lamina strength index; T_1 is the tensile strength of the lamina; T_r is the tensile strength of the shale reservoir. Three

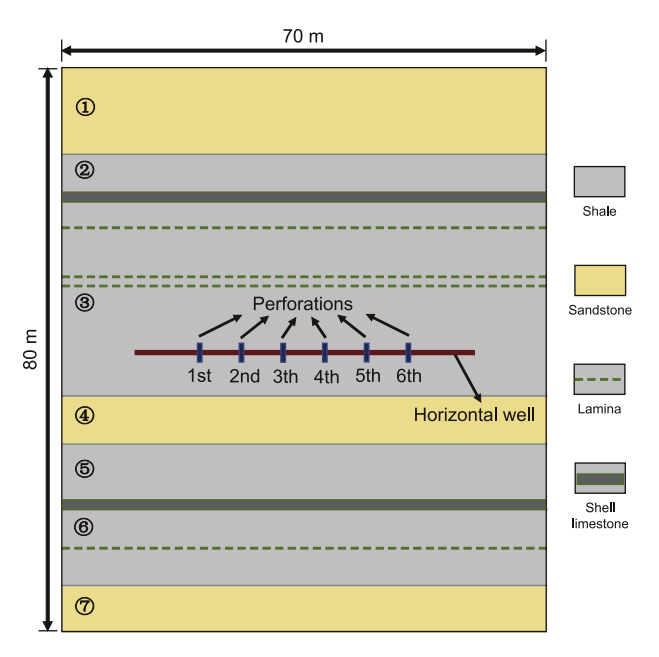


Fig. 4. Numerical model schematic.

sets of experiments were set up, and the γ_1 was 0.4, 0.5, and 0.6, respectively. Fig. 4 represents a 70 m \times 80 m computational domain for multi-cluster cross-layer numerical simulation, which included a horizontal wellbore, twelve perforation holes. The model was discretized into a fully saturated porous domain with CPE4P elements. The discretized model with 103,431 nodes and 61,902 elements.

The whole model was divided into 7 layers, layers 2, 3, 5, 6 were interspersed with shell limestone interlayers, and several lamina were set in the shale layer. The specific simulation parameters are shown in Table 1.

Considering the three variables of cluster spacing, pump rate, and lamina strength, a multi-cluster cross-layer numerical model was established to explore the unbalanced multi-fracture propagation and longitudinal penetration law of Lianggaoshan Formation continental shale formation in Sichuan Basin.

3. Numerical results and analysis

3.1. Effect of lamina strength on hydraulic fracture propagation

The geological structure of Lianggaoshan Formation is complex, the rock mechanical properties of lamina and shell limestone interbed are quite different. As shown in Fig. 4, five shale laminas are set according to the site geology, and two shell limestone layers are located in the shale reservoir. As shown in Fig. 5, in the case of

Table 1The parameters of the numerical model.

Simulation parameter	Value
Young's modulus, GPa	30-51
Poisson's ratio	0.24-0.30
Maximum horizontal stress, MPa	72.6
Minimum horizontal stress, MPa	65.9
Vertical stress, MPa	70.1
Porosity, %	0.1
Fracturing fluid viscosity, mPa·s	15
Number of perforations per cluster	2
Pump rate, m ³ /min	2/10/18

6 m cluster spacing, the fractures can effectively communicate with the central lamina, but due to the strong plasticity characteristics of the mesoscopic tuff strips with high compressive and elastic modulus, the fractures are difficult to break through effectively.

When the cluster spacing is 6 m, the 3rd and 4th fractures in the central are seriously affected by the stress shadow effect, showing a nearly unidirectional propagation trend. Increasing the lamina strength, the lamina activation effect of the fractures is improved, and the height growth of the fractures is more favorable. 6 m cluster spacing conditions all show an obvious unbalanced propagation phenomenon between the fractures, and only the sandstone-shale interface between the 3 and 4 layers is activated. When the lamina strength index is 0.6, the fractures cross upwards to the upper part of layer 5 and downwards to layer 2, resulting in a better cross-layer effect.

The fractures communicate two laminas and activate three sandstone-shale interfaces at low lamina strength when the cluster spacing is increased to 7 m and lamina strength index is 0.5 (Fig. 6(b)). As the lamina strength increased, the fractures tended to propagate in the direction of the fracture height without activating the lamina in the shale, and only activated one to two interfaces. The outer side fractures are not restricted to propagate in the vertical stress direction, and the deflection angle is small. When the lamina strength is small, the pore pressure around the fracture opening and at the activated lamina is high.

Hydraulic fractures activated four lamina and interlayer interfaces when the cluster spacing increased to 8 m at a grain layer strength of 0.4. As the lamina strength was increased to 0.5, the fracture propagation was hindered and the number of interlayer interfaces communicated 2 laminas and 1 sandstone-shale interface. As the lamina strength further increases, the fracture height did not increase due to the large cluster spacing and the limited liquid energy for the longitudinal propagation of the fracture system, and only one lamina is activated (Fig. 7(c)). The high pore pressure region is larger when the striatal layer strength is lower, indicating a better reservoir modification effect. When the hydraulic fracture activates more lamina, the phenomenon of non-uniform propagation of the hydraulic fracture is more obvious, which leads to the non-symmetric pore pressure disturbance area on both sides of wellbore.

Fig. 8 demonstrates the maximum fracture width versus the total height of the fracture system for different lamina strength indices at 8 m cluster spacing conditions. The maximum width of the fracture is opposite to the variation trend of the fracture height, and the growth rate of the fracture width is different under the condition of different lamina strength index. Due to the large initial liquid energy, a large fracture width can be achieved in a short period of time when the lamina strength index is high, so its change over time was small.

At a cluster spacing of 9 m and lamina strength index is 0.6 (Fig. 9(c)), the fracture system had no significant increase in fracture height, but the activation efficiency of the interface was reduced. With lamina strength index is 0.4 (Fig. 9(a)), the fracture activated two laminas and one interlayer interface, the fracture height did not decrease compared with the other control groups, and the fracturing effect was better. It is worth noting that the fractures on both sides are dominant in the initial propagation. They always activate and communicate the interface structure first, resulting in insufficient subsequent fluid energy and limited growth of height.

When the cluster spacing is 10 m, the lower lamina strength tends to activate more lamina, and the fracture unbalanced propagation phenomenon is not obvious. When increasing the lamina strength to 0.5 (Fig. 10(b)), two interfaces at the same height were activated but not communicated, and the stress interference effect

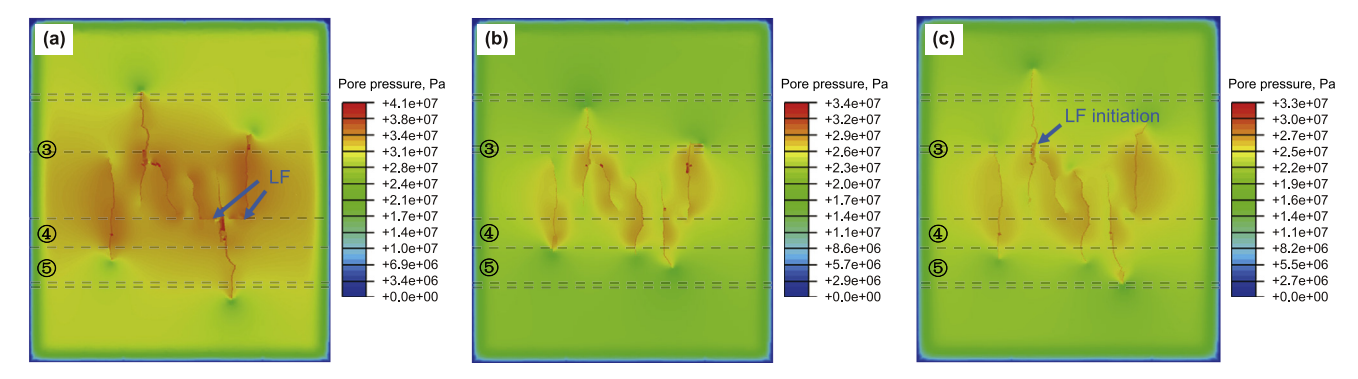


Fig. 5. Pore pressure contours at different lamina strength as the cluster spacing is 6 m: (a) Lamina strength index is 0.4; (b) Lamina strength index is 0.5; (c) Lamina strength index is 0.6. In the figure, LF denotes lamina fracture.

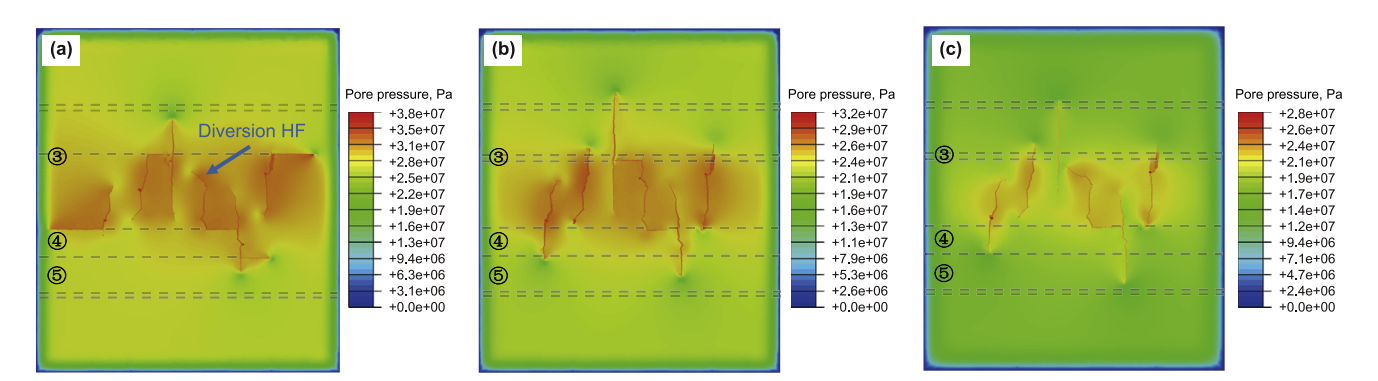


Fig. 6. Pore pressure contours at different lamina strength as the cluster spacing is 7 m: **(a)** Lamina strength index is 0.4; **(b)** Lamina strength index is 0.5; **(c)** Lamina strength index is 0.6. In the figure, HF denotes hydraulic fracture.

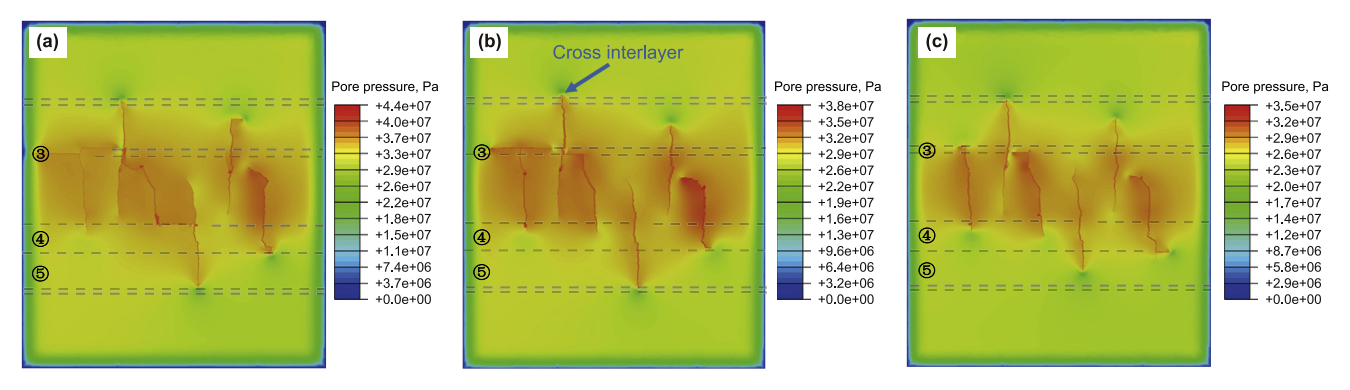


Fig. 7. Pore pressure contours at different lamina strength as the cluster spacing is 8 m: (a) Lamina strength index is 0.4; (b) Lamina strength index is 0.5; (c) Lamina strength index is 0.6

between fractures led to the unbalanced propagation phenomenon. The maximum pore pressure did not change when the lamina strength increased to 0.6, but the fracture heights all decreased, and the ripple range of the fracture system was smaller, which was not conducive to the strength of the layer as a fracture target. In the numerical simulation results of this section, it was found that the fractures in the near-wellbore section appear to attract each other, which will lead to the deflection of the fracture tip stress at $\sigma_{\rm h}$, thus affecting the penetration ability of the hydraulic fractures, which is not conducive to the longitudinal reformation of the reservoir.

It is important to ensure the propagation efficiency of each cluster of fractures. For the geological structure of thin interlayer of laminated shale and the development of lamina, it is recommended

to select the layer with moderate cementation strength of lamina for fracturing modification to improve the chance of forming complex fracture network.

3.2. Effect of pump rate on hydraulic fracture propagation

The construction pump is a key factor affecting the effect of hydraulic fracturing transformation.

Fig. 11 shows the trend of the fracture height of each cluster at 8 m cluster spacing for different pump rate. Under the same cluster spacing, increasing the pump rate can effectively improve the transformation level of the formation. It can be found that the fracture heights of fractures 2 and 5 are larger only at the discharge

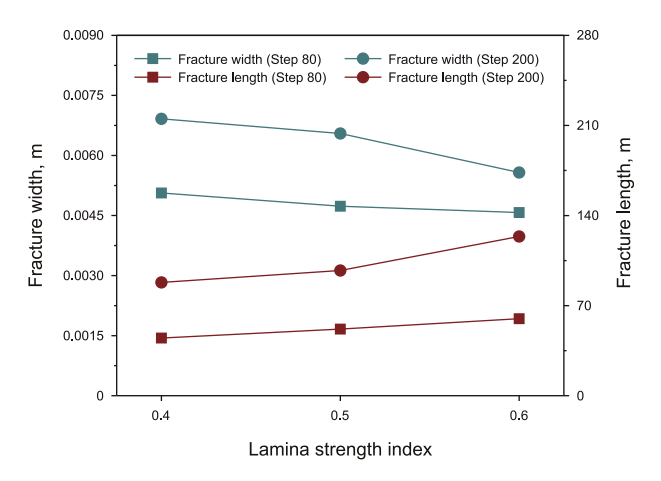


Fig. 8. Fracture width and total fracture height under different lamina strength conditions.

rate of 2–10 m³/min, indicating that they are dominant in the unbalanced fracture propagation, and the height of the rest of the fractures are roughly around 10 m. Increasing the discharge volume to 18 m³/min, the growth rate of fracture height generally increases, while the growth value of fracture height of 5th fracture is the lowest. It can be found in Fig. 1 that due to the effect of interfracture stress shadowing and insufficient intra-fracture pressure, it activates the interface of small layer 5 during propagation, thus limiting its height. It can be seen that high pump rate can effectively increase the height of the fracture system, but attention still needs to be paid to the competing propagation factors between fractures.

Increasing the pump rate can effectively improve the drainage range and achieve the purpose of increasing production and efficiency.

3.3. Study the effect of cluster spacing on hydraulic fracturing propagation based on AE technique

Cluster spacing is an important design parameter for multicluster fracturing of horizontal wells. The cluster spacing is too large to reduce the reservoir transformation scale and affect the production enhancement effect. The cluster spacing is too small to increase the stress interference between fractures, which has a great influence on fracture propagation and FSA (fracture surface area). This section focuses on the effect of fracture spacing on the propagation and morphology of multi-fractures. To visually demonstrate the fracture pattern and the lamina communication morphology, the fracture pattern occupancy ratio was extracted and plotted on the plate, and the color of each point represents the ratio of tensile damage to shear damage in the fracture, as well as the damage of fracture pattern reconstruction at the lamina.

The mode composite ratio *MMIXDME* during cohesive element damage is extracted to more clearly describe the fracture evolution mechanism of the fracture during fracturing, and the parameters are defined as follows:

$$MMIXDME = 1 - m_1 \tag{12}$$

$$m_1 = \frac{G_{\rm n}}{G_{\rm T}} \tag{13}$$

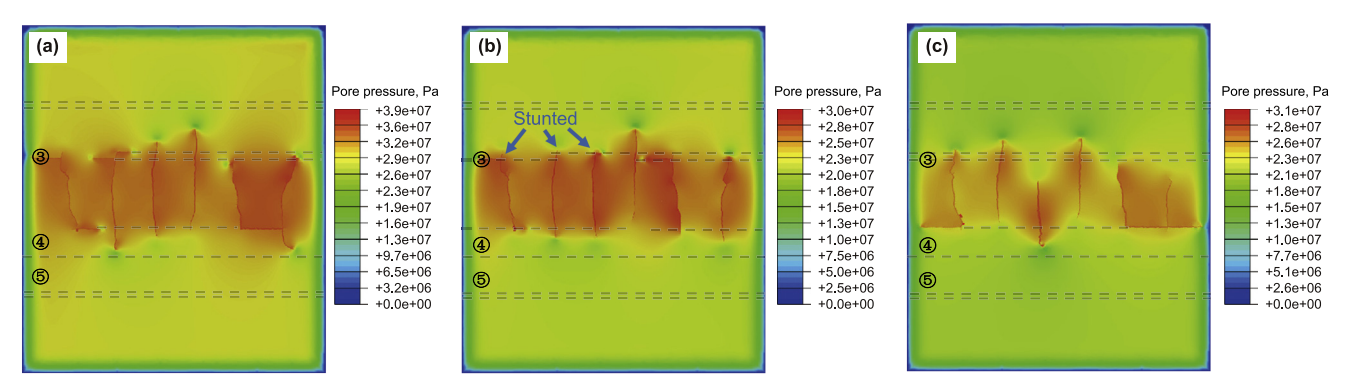


Fig. 9. Pore pressure contours at different lamina strength as the cluster spacing is 9 m: (a) Lamina strength index is 0.4; (b) Lamina strength index is 0.5; (c) Lamina strength index is 0.6.

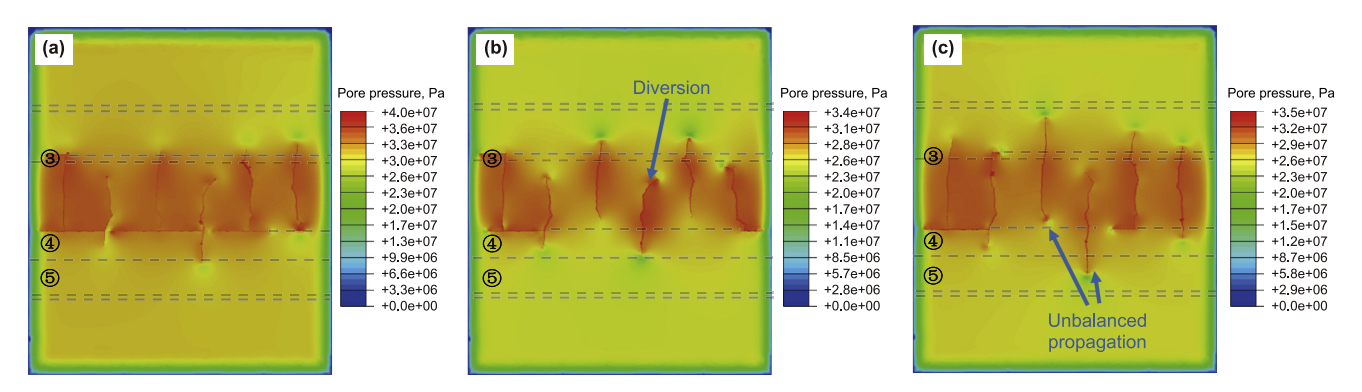


Fig. 10. Pore pressure contours at different lamina strength as the cluster spacing is 10 m: (a) Lamina strength index is 0.4; (b) Lamina strength index is 0.5; (c) Lamina strength index is 0.6.

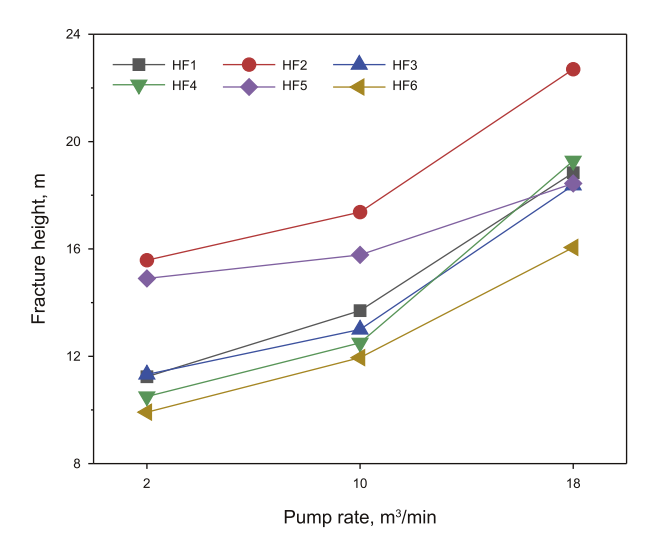


Fig. 11. The height of each fracture when the cluster spacing is 8 m and the pump rates are $2, 10, 18 \text{ m}^3/\text{min}$, respectively.

$$G_{\mathsf{T}} = G_{\mathsf{S}} + G_{\mathsf{t}} + G_{\mathsf{n}} \tag{14}$$

where m_1 represents the proportion of the fracture energy of mode I fracture; G_n , G_s , and G_t represent the fracture energies in the normal and two shear directions, respectively; MMIXDME = 1 represents a shear fracture, MMIXDME = 0 represents a tension fracture, and MMIXDME between 0 and 1 represents Tensile-shear mixed fractures.

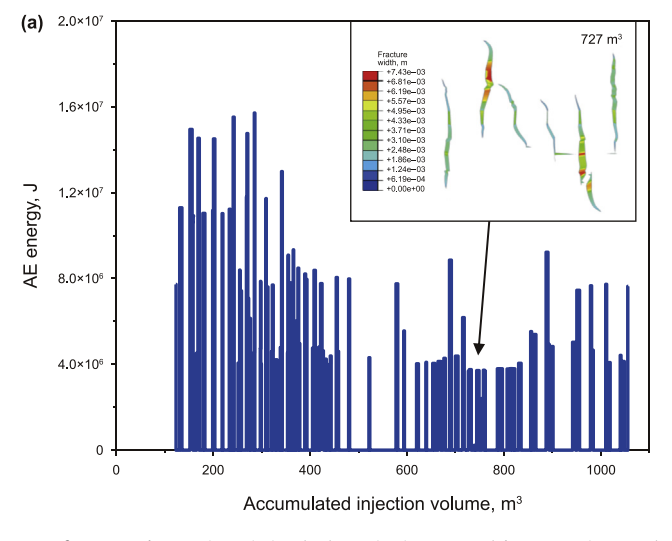
Acoustic emission (AE) technique is an efficient fracture monitoring method, which can be used to monitor the fracture propagation and location coordinates in hydraulic fracturing in full-time domain and provide an effective reference for fracturing evaluation analysis. The numerical simulation results are extracted by Python, and the fracturing simulation results are processed and analyzed based on the principle of AE method. The energy and number of times of damage generated at different locations of the formation under the same moment were extracted, and the energy of acoustic emission at each moment was calculated. The number of damaged elements at all moments of the fracturing process was taken as the number of acoustic emission events.

When the cluster spacing is 6 m, the energy distribution of fracturing fluid is more concentrated at fracture initiation, and the AE curve shows a higher energy at the initial stage and the highest energy reaches 1.6×10^7 power at 292 m³ (Fig. 12(a)). When the accumulated injection volume reaches 727 m³, the AE energy is lower and uniformly distributed. The fracture morphology diagram reveals that the hydraulic fracture activates the weak surface of sandstone and shale cementation at this time, and the lower interfacial strength leads to a lower AE energy at its rupture. 2nd and 5th fractures are dominant in propagation and break through the strongly plastic shell limestone interlayers. Fractures will propagate when the deformation energy released by fracture propagation is equal to or greater than the increase in surface energy due to the formation of a new free surface.

Fig. 13 shows the AE energy profile with fracture mode reconstruction when the cluster spacing of 7 m. The fracture initiation pattern is similar to that at 6 m. The AE energy fluctuation when the accumulated injection volume was between 312 m³ to 525 m³ is drastic representing the obvious phenomenon of fracture unbalanced propagation and accompanied by the phenomenon of multiple fractures cross the layers. When the accumulated injection volume near 692 m³, the fractures propagation in two directions along the main fracture and lamina, and the AE energy curve fluctuated greatly and was accompanied by the appearance of weak-signal time points. The percentage of shear damage of lamina fractures on both sides increases significantly.

When the cluster spacing increases to 8 m (Fig. 14), the fluctuation range of the AE energy curve decreases and the number of activations at the lamina and sandstone-shale interfaces increases. The overall AE energy is lower, indicating that less energy is required for fracture opening and propagation. The fracture initiation must overcome both the in-situ stress field and the interference stress field caused by the stress shadow, which leads to significant fracture steering in the middle. In the post-fracture stage, due to the rapid propagation and coalescence of the fracture, coupled with the shear friction between the shear fracture surfaces, the internal strain energy of the specimen is rapidly released, resulting in a rapid release of the internal strain energy of the specimen and a sharp increase in acoustic emission energy, which shows a jump and reaches a peak.

When the cluster spacing is 9 m (Fig. 15), the AE energy fluctuation in the early stage is large, which responds to the high rate of fracture propagation along the vertical direction. The interference



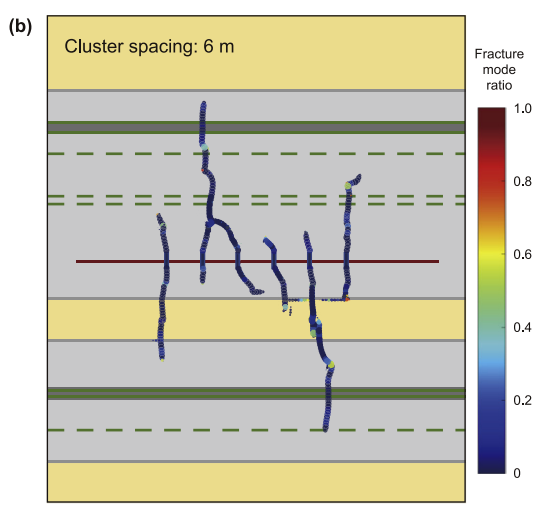


Fig. 12. Fracture feature and acoustic emission (AE) monitoring curves (cluster spacing: 6 m): (a) AE energy distributions; (b) Fracture mode reconstruction of fracture paths.

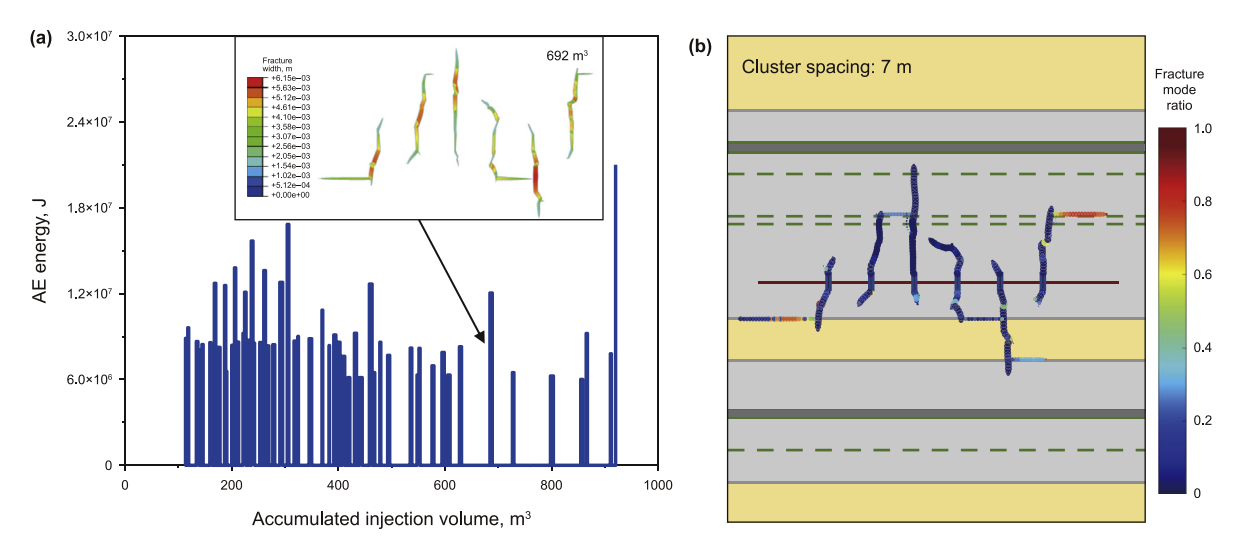


Fig. 13. Fracture feature and AE monitoring curves (cluster spacing: 7 m): (a) AE energy distributions; (b) Fracture mode reconstruction of fracture paths.

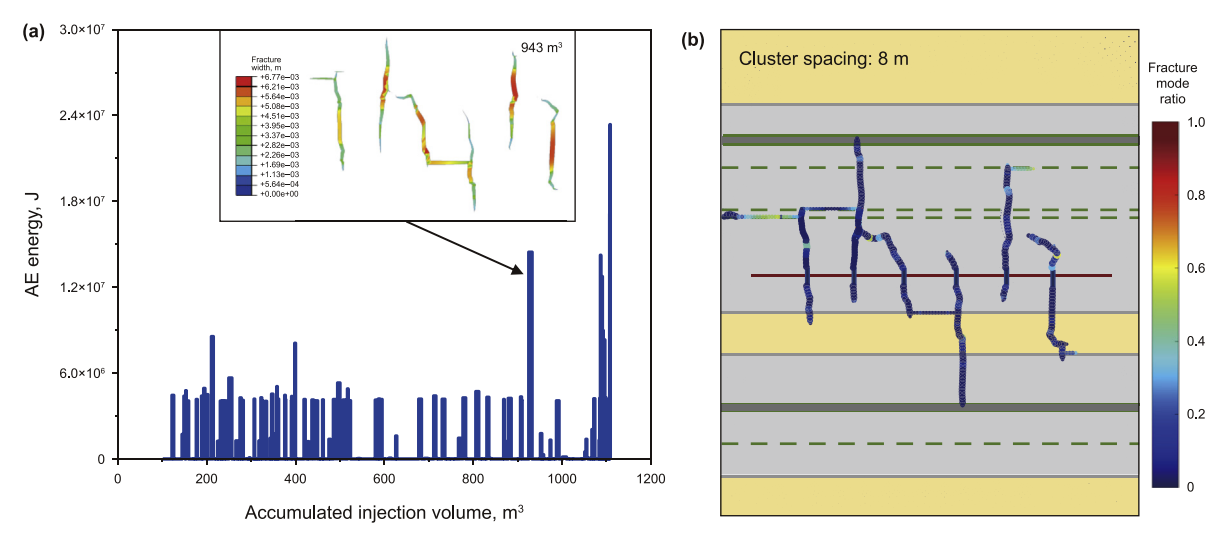


Fig. 14. Fracture feature and AE monitoring curves (cluster spacing: 8 m): (a) AE energy distributions; (b) Fracture mode reconstruction of fracture paths.

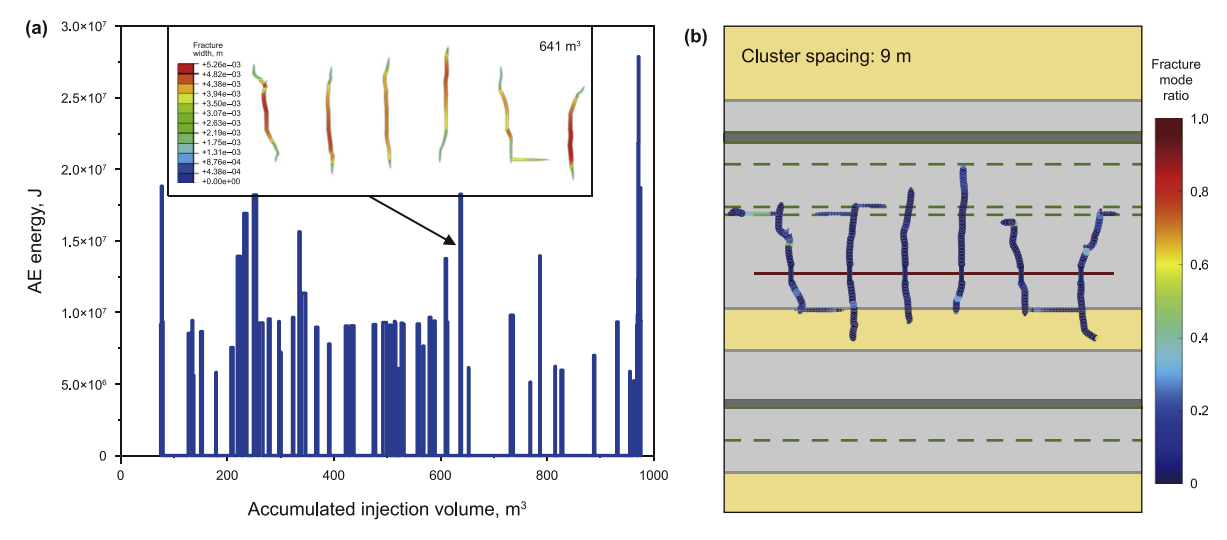


Fig. 15. Fracture feature and AE monitoring curves (cluster spacing: 9 m): (a) Acoustic emission (AE) energy distributions; (b) Fracture mode reconstruction of fracture paths.

phenomenon between the fractures in the early stage is not obvious and does not activate the lamina by Fig. 15(b). When the accumulated injection volume near 641 $\rm m^3$, the fractures first activated the sandstone-shale interface, at which time most of the fractures continued to propagate along the vertical lamina direction. After accumulated injection volume reached 662 $\rm m^3$, the striated layers were also activated one after another, and the AE energy decreased rapidly, finally the left fracture propagated to the boundary of the formation.

When the cluster spacing increases to 10 m (Fig. 16), the height of fracture in each cluster is similar and the unbalanced propagation of the fracture system is not obvious. The stress interference between fractures decreases with the increase of cluster spacing. The fracture deflection angle decreases with increasing cluster spacing, indicating that the stress shadow between different induced fractures decreases with increasing cluster spacing. 10 m cluster spacing tends to activate the lamina interface with similar depth, and increasing cluster spacing is not conducive to the formation of complex fracture network.

The maximum value of AE energy appears at the post-hydraulic fracturing stage and increases with the increase of cluster spacing. Due to the increase of cluster spacing, the fracture propagated rapidly in the late stage and the stress interference between the fractures is not concentrated, which leads to the increase of AE energy.

Fig. 17 is plotted according to the trend of AE events and tensile-shear percentage under different cluster spacing. The proportion of fracture mode of fractures is less affected by the cluster spacing, while the overall trend of total AE counts is increased. The percentage of shear damage at cluster spacing of 6 m is the highest, and the number of shear damage as dominant is 0. The percentage of shear damage increases at cluster spacing of 7 m. Combined with Fig. 5, the part of shear damage as dominant is mainly distributed in the outer lamina and layers interface, and the fracture pattern is more complex.

The cluster spacing has a significant effect on the fracture propagation height and morphology. The overall trend of fracture length decreases with increasing cluster spacing, while the activation efficiency of the lamina gradually increases. The percentage of tensile fracture of fractures was higher, while the percentage of shear fracture of fractures in the lamina increased. When the cluster spacing is 9 and 10 m, the main fractures as a whole are almost parallel to the maximum horizontal principal stress.

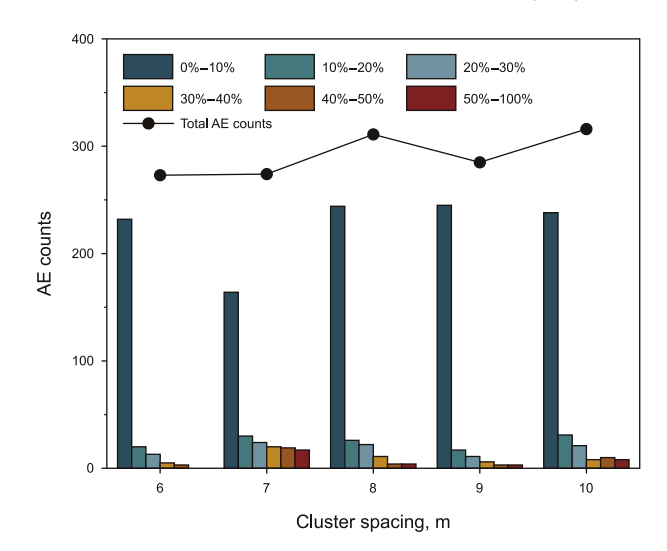
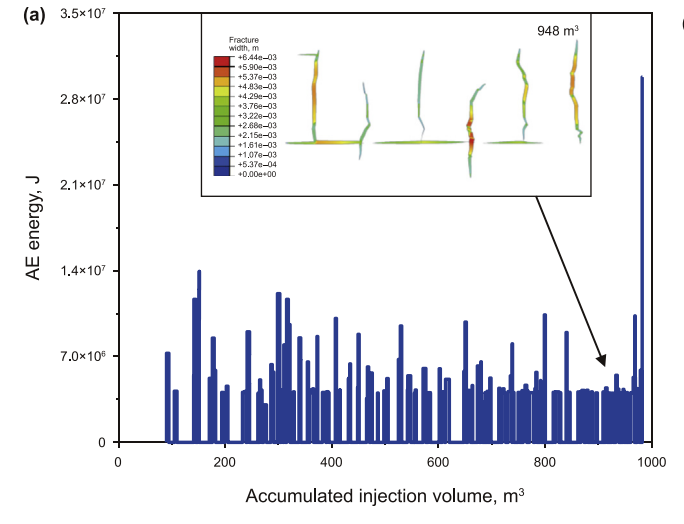


Fig. 17. AE counts and ratio of tensile damage to shear damage in the fracture under different cluster spacing.

The histogram of the fracture height of each cluster under different cluster spacing conditions was plotted (Fig. 18). It can be found that when the cluster spacing is small, the fractures on both sides are more likely to activate the lamina or interlayer interface, and as the cluster spacing increases to 8 m, the gap in fracture height decreases, the number of fracture-activated interfaces is more, and the overall penetration effect is better. When the cluster spacing continues to increase, the number of fracture-activated interfaces decreases, even though the interstitial stress shadow effect is weakened, but the overall penetration effect is average. When the lamina strength is higher, the communicated lamina and interlayer interfaces are generally less, but the fracture height increases. It is important to preferably select the fracture layer target (Li and Wu, 2022b). When the perforation section is located in a layer with high plasticity and high elastic modulus and compressive strength, the discharge volume can be appropriately increased and the cluster spacing can be reduced to increase the fracture height as the main purpose, which can improve the chance of complex fracture formation.



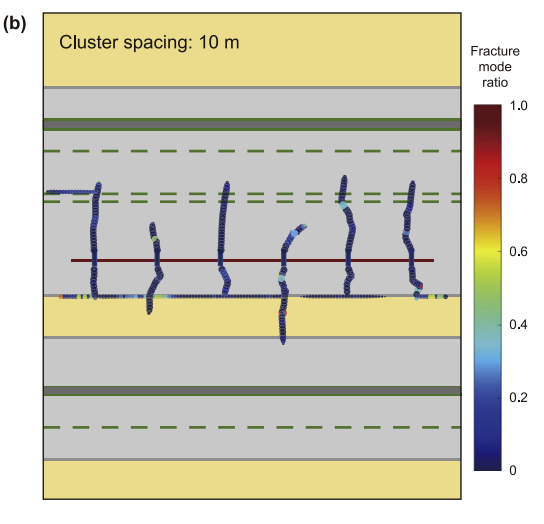


Fig. 16. Fracture feature and AE monitoring curves (cluster spacing: 10 m): (a) AE energy distributions; (b) Fracture mode reconstruction of fracture paths.

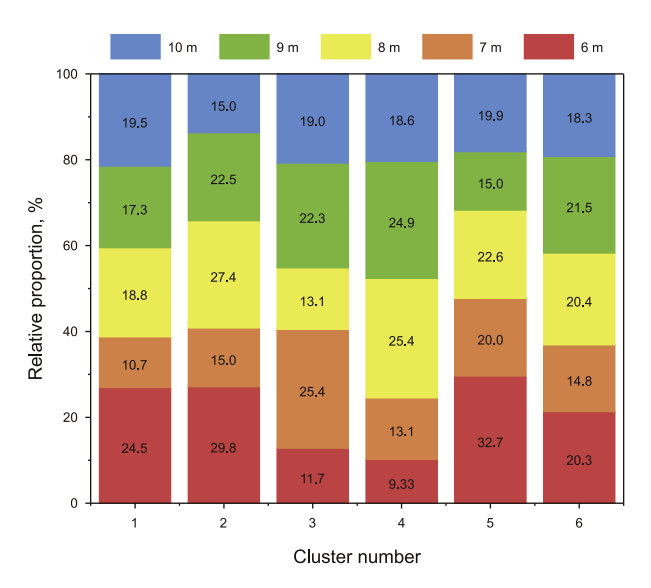


Fig. 18. The histogram of the fracture height of each cluster under different cluster spacing conditions.

4. Discussion

In this paper, the unbalanced propagation of fractures and their layer penetration patterns under multi-cluster conditions were analyzed. The height of fractures and the number of activated laminas directly reflect the complexity of the fracture system. It can be more intuitive to study the variation law of discharge volume and cluster spacing during the whole fracturing process. Meanwhile, in the study of multi-fracture unbalanced propagation, lamina strength index is proposed to quantify the strength difference of fractured layers, which is important for guiding the design

of multi-fracture cross-layer fracturing.

From the numerical simulation analysis described, we found that in the laminated sandstone-shale interbedding formation, there are four basic modes of hydraulic fracture and lamina. As shown in Fig. 19(a), when the cluster spacing is close, the fracture ends gradually turns slightly, the bedding is not activated, and only one fracture is perpendicular to the vertical stress. As shown in Fig. 19(b), the propagation of a certain fracture is in the ascendant position, resulting in greater stress shadow effect on adjacent fracture. The fracture mode is similar to En échelon fracture is illustrated in Fig. 19(e). It is commonly observed in geology, induced by a mechanical interaction between their near-tip stress fields (Li et al., 2020). The fracture turns when it does not reach the lamina, which is similar to the behavior between fractures in sandstone. If the cluster spacing is too large (Fig. 19(c)), the dominant fracture will open a certain lamination first. Since the energy of the fluid in the fracture cannot activate more laminations, the subsequent fractures tend to activate the same lamination, and the fracturing fluid is more likely to leak along the bedding. As illustrated in Fig. 19(d), the cluster spacing and lamination strength are moderate, the fracture can activate more laminations, and the stepped fracture are easy to appear, improved the fracture complexity. As shown in Fig. 19 (side view), hydraulic fracturing experiments were conducted on the downhole core, several laminas were activated in the path of HF (hydraulic fracture) propagation, and some of them were in an incomplete activated state (see Fig. 20).

Based on the numerical model, it was compared with the experimental results of hydraulic fracturing. Shale outcrops of the Jurassic Lianggaoshan Formation in Sichuan Basin were selected for hydraulic fracturing experiments. The fractures already showed unbalanced propagation behavior before encountering the structural weak surface such as the lamina, and deflection occurred when the dominant fracture encountered the weak surface, which was not necessarily completely parallel to the weak surface and the

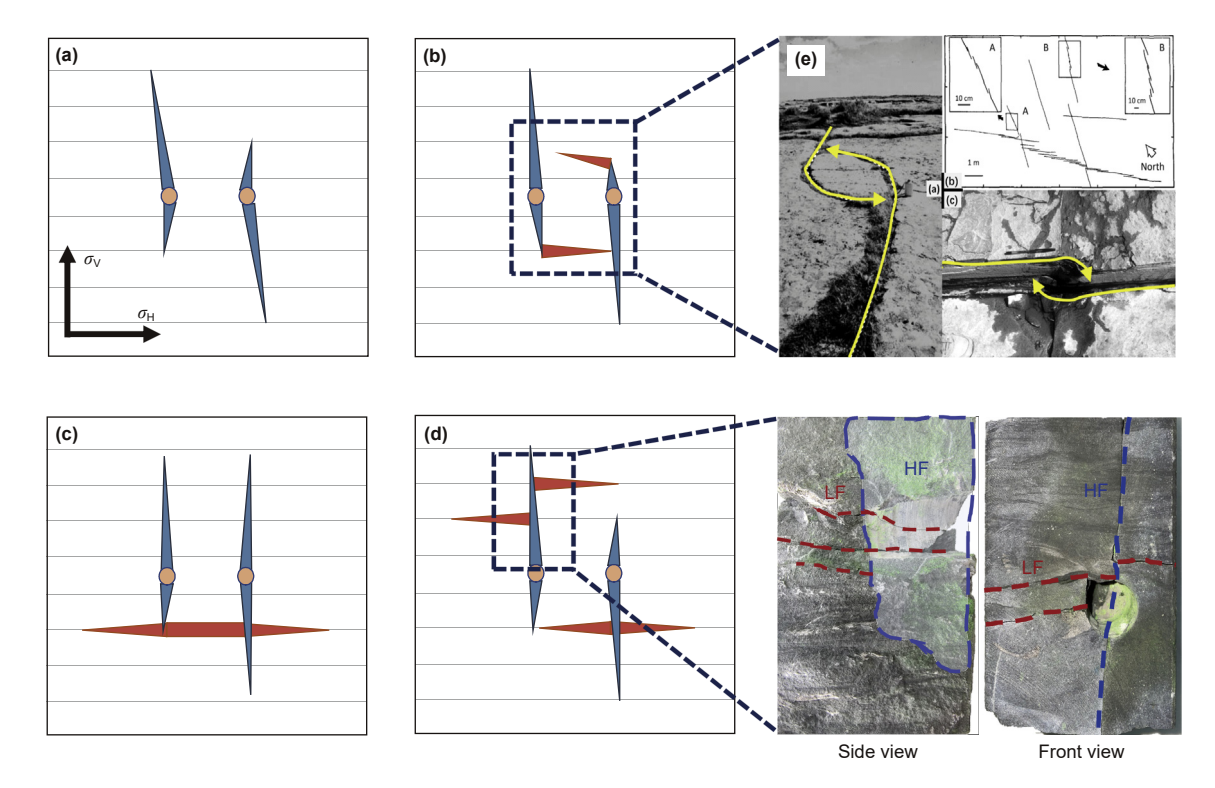
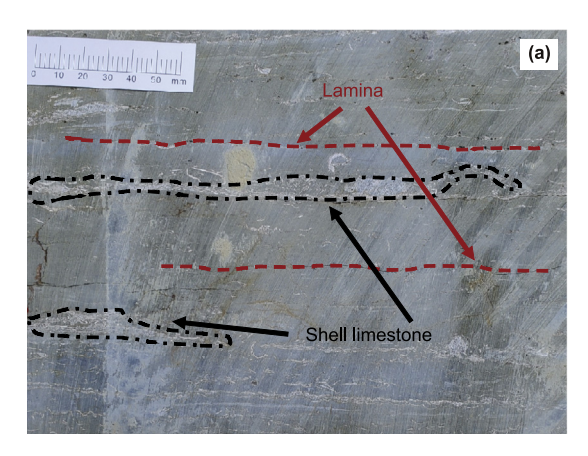


Fig. 19. Model of multiple hydraulic fractures initiation and propagation. (a) Repulse arch fracture; (b) and (e) En échelon fracture (Li et al., 2020); (c) T-shaped fracture; (d) Fishbone-like fracture.



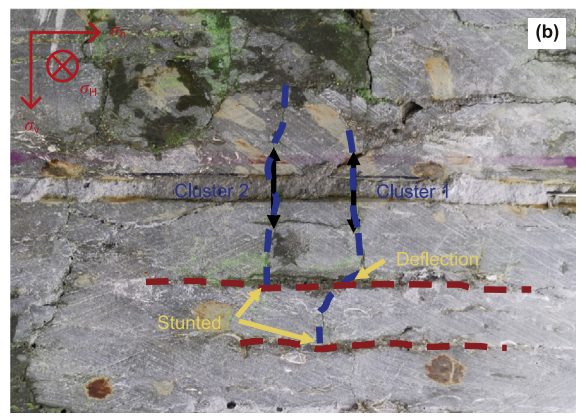


Fig. 20. (a) Interbedded sandstone-shale specimen for fracturing experiment; (b) Fracture morphologies of specimen.

phenomenon also consistent with the numerical simulation results of this paper (Fig. 12(b)).

The model constructed in this paper assumes that the fracturing fluid is injected into the formation from each perforation. However, during staged fracturing of horizontal wells, the actual fracturing fluid flows from the wellhead into each perforation and then into the formation, and the perforation entry friction affects the fracture initiation and propagation behavior, which has a greater impact on the distribution of the subsequent fracturing fluid flow.

A large number of current studies only consider the effect of fluid partitioning or composition of different layers and lack the combination of both. Therefore, this study adds a tubular flow element to the numerical model in the previous section to analyze the flow partitioning phenomenon in the wellbore on hydraulic fracture initiation and propagation.

It can be seen by Fig. 21 that the fractures on the outer side were in the competition in the pre-fracturing period with larger widths. The width of the 3rd fracture is the smallest and increases with fracturing time, the 3rd fracture finally closes due to the joint effect of stress interference effect of both sides of the fracture and perforation entry friction. When the cumulative liquid injection volume is 500 m³, the width of the fractures on both sides is much larger than that of the inner fractures, and the unbalance propagation phenomenon is more obvious. When coupling the wellbore

and considering the dynamic distribution of fracturing fluid, the resistance of the fracture system increased, leading to serious energy loss of fracturing fluid, which did not effectively penetrate more reservoirs and only activated the upper shale lamina and sandstone-shale interface. Li et al. (2017) developed a threedimensional multicluster fracturing model considering the dynamic distribution of flow to investigate the simultaneous growth of multiple fractures during fracturing. The results show that a sufficiently large injection pressure drop can offset the stress shadow between multiple fractures and help equalize the length of multiple fractures. However, formations are distributed with a large number of interlayer interfaces, and it is important to consider the study of multiple fracture propagations in geological structures such as lamina. How to improve the number and efficiency of fracture penetration within the same fracturing parameters is the focus of research on multi-cluster fracturing in horizontal wells.

5. Conclusions

In this paper, a series of experimental studies on multi-cluster cross-layer fracturing in horizontal wells were conducted on the terrestrial shales of the Lianggaoshan Formation in the Sichuan Basin, explored the relationship between fracture interactions. Primary conclusions are as follows.

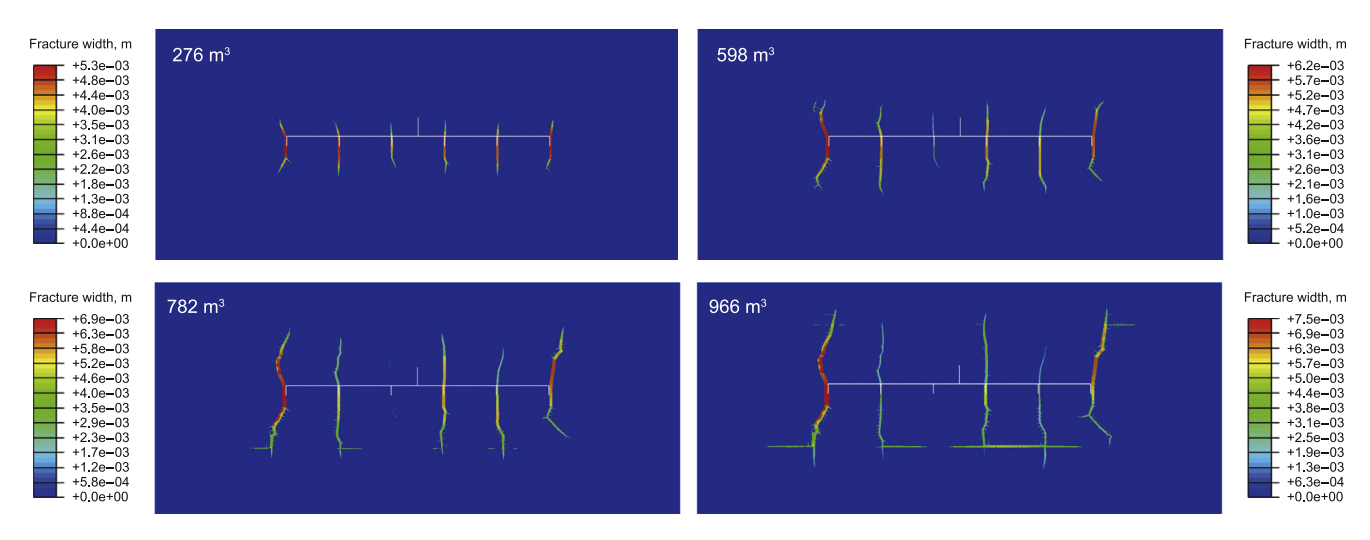


Fig. 21. Fracture width of six fractures at different time.

- 1) The phenomenon of unbalanced propagation of multiple fractures will seriously restrict the production increase effect after fracturing, the difference of fracture propagation rate of each fracture will decrease with the increase of cluster spacing, the middle fractures are generally at a disadvantage in propagation, and reasonable setting of cluster spacing can reduce the stress shadow effect between fractures and improve the fracture area. Increasing the pump rate can effectively increase the fracture longitudinal penetration ability and open more lamina and interfaces based on increasing the fracture height.
- 2) The fracture damage evolution analysis based on AE parameters can study the damage process of the rock from mesoscopic. When the fracture is pressure-holding, the change of AE energy is small, and when the fracture propagates in the vertical stress direction, the peak of AE energy increases significantly. Tensile fracture accounts for a higher percentage of fracture propagation through the layer, while shear fracture mainly occurs during the activation of the lamina and fracture turning.
- 3) There are four types of multi-fracture interaction behavior in laminated shale reservoirs: (a) back-to-back-like fractures; (b) En échelon-like fractures (activation of partially lamina); (c) multiple fractures activating the same lamina; (d) multi-fracture activation of multiple lamina.
- 4) Aiming at the geological structure of multiple interbeds and lamina in the Lianggaoshan Formation, it is necessary to set the fracture target location reasonably. The layer with low lamina strength is good for fracture propagation along the interface, but it will attenuate the distance of fracture propagation in height. The site fracturing design can increase the discharge volume above 18 m³/min, increase the number of injection holes in the section and set the cluster spacing at 8 m to achieve the purpose of effectively transforming the terrestrial shale reservoir.

Data availability statement

All data that support the findings of this study are included in the manuscript.

CRediT authorship contribution statement

Jia-Xin Lv: Formal analysis, Investigation, Software, Validation, Visualization, Writing — original draft. **Bing Hou:** Conceptualization, Data curation, Funding acquisition, Methodology, Project administration, Resources, Supervision, Writing — review & editing.

Declaration of competing interest

The authors declare that they have no known competing financial interests or personal relationships that could have appeared to influence the work reported in this paper.

Acknowledgments

The authors are grateful for the financial support by the National Key Research and Development Program of China (No. 2022YFE0129800) and the National Natural Science Foundation of China (No. 52074311).

References

- Chang, Z., Hou, B., 2022. Numerical simulation on fractured shale oil reservoirs multi-cluster fracturing under inter-well and inter-cluster stress interferences. Rock Mech. Rock Eng. 1–17. https://doi.org/10.1007/s00603-022-03145-7.
- Chen, M., Zhang, S.C., Xu, Y., et al., 2020. A numerical method for simulating planar 3D multi-fracture propagation in multi-stage fracturing of horizontal wells.

- Chen, X.Y., Li, Y.M., Zhao, J.Z., et al., 2018. Numerical investigation for simultaneous growth of hydraulic fractures in multiple horizontal wells. J. Nat. Gas Sci. Eng. 51, 44–52. https://doi.org/10.1016/ji.jingse.2017.12.014.
- Cheng, Y., 2012. Impacts of the number of perforation clusters and cluster spacing on production performance of horizontal shale-gas wells. SPE Reservoir Eval. Eng. 15 (1), 31–40. https://doi.org/10.2118/138843-PA.
- Diehl, T., 2008. On using a penalty-based cohesive-zone finite element approach, part I: Elastic solution benchmarks. Int. J. Adhesion Adhes. 28 (4), 237–255. https://doi.org/10.1016/j.ijadhadh.2007.06.003.
- Dontsoy, E.V., Suarez-Rivera, R., 2020. Propagation of multiple hydraulic fractures in different regimes. Int. J. Rock Mech. Min. 128, 104270. https://doi.org/10.1016/i.iirmms.2020.104270.
- Han, W.G., Cui, Z.D., Zhang, J.Y., 2020. Fracture path interaction of two adjacent perforations subjected to different injection rate increments. Comput. Geotech. 122, 103500. https://doi.org/10.1016/j.compgeo.2020.103500.
 Hossain, M.M., Rahman, M.K., 2008. Numerical simulation of complex fracture
- Hossain, M.M., Rahman, M.K., 2008. Numerical simulation of complex fracture growth during tight reservoir stimulation by hydraulic fracturing. J. Pet. Sci. Eng. 602 (2), 86–104. https://doi.org/10.1016/j.petrol.2007.05.007.
- Hou, B., Chang, Z., Fu, W.N., et al., 2019. Fracture initiation and propagation in a deep shale gas reservoir subject to an alternating—fluid—injection hydraulic fracturing treatment. SPE J. 24 (4), 1–17. https://doi.org/10.2118/195571-PA.
- Hou, B., Zhang, Q.X., Liu, X., et al., 2022. Integration analysis of 3D fractures network reconstruction and frac hits response in shale wells. Energy 260, 124906. https://doi.org/10.1016/j.energy.2022.124906.
- Jin, X., Li, G.X., Meng, S.W., et al., 2021. Microscale comprehensive evaluation of continental shale oil recoverability. Petrol. Explor. Dev. 48 (1), 222–232. https:// doi.org/10.1016/S1876-3804(21)60021-6.
- Jin, Z.J., Zhu, R.K., Liang, X.P., et al., 2021. Several issues worthy of attention in current lacustrine shale oil exploration and development. Petrol. Explor. Dev. 48 (6), 1276–1287. https://doi.org/10.1016/S1876-3804(21)60303-8.
- Lecampion, B., 2009. An extended finite element method for hydraulic fracture problems. Commun. Numer. Methods Eng. 25 (2), 121–133. https://doi.org/10.1002/cnm.1111.
- Li, J.W., Li, Y.C., Wu, K., 2021. An efficient higher order displacement discontinuity method with joint element for hydraulic fracture modeling. In: ARMA US Rock Mechanics/Geomechanics Symposium. ARMA-2021-1301.
- Li, J.W., Liu, Y.Z., Wu, K., 2022. A new higher order displacement discontinuity method based on the joint element for analysis of close-spacing planar fractures. SPE J. 27 (2), 1123–1139. https://doi.org/10.2118/208614-PA.
- Li, J.W., Wu, K., 2022a. An efficient model for hydraulic fracture height growth considering the effect of bedding layers in unconventional shale formations. SPE J. 27 (6), 3740–3756. https://doi.org/10.2118/210572-PA.
- Li, J.W., Wu, K., 2022b. Impact of horizontal weak interfaces on the hydraulic fracturing: from height growth to lateral propagation. In: SPE/AAPG/SEG URTEC. D021S032R003. https://doi.org/10.15530/urtec-2022-3723910.
- Li, S.B., Firoozabadi, A., Zhang, D.X., 2020. Hydromechanical modeling of nonplanar three-dimensional fracture propagation using an iteratively coupled approach.
 J. Geophys. Res. Solid Earth 125 (8), e2020JB020115. https://doi.org/10.1029/2020JB020115.
- Li, Y., Deng, J.G., Liu, W., et al., 2017. Numerical simulation of limited-entry multicluster fracturing in horizontal well. J. Petrol. Sci. Eng. 152, 443–455. https:// doi.org/10.1016/j.petrol.2017.03.023.
- Liu, W.Z., Zeng, Q.D., Yao, J., 2018. Numerical simulation of elasto-plastic hydraulic fracture propagation in deep reservoir coupled with temperature field. J. Petrol. Sci. Eng. 171, 115–126. https://doi.org/10.1016/j.petrol.2018.07.041.
- Liu, X., Rasouli, V., Guo, T.K., et al., 2020. Numerical simulation of stress shadow in multiple cluster hydraulic fracturing in horizontal wells based on lattice modelling. Eng. Fract. Mech. 238, 107278. https://doi.org/10.1016/j.engfracmech.2020.107278.
- Lu, W.Y., He, C.C., 2022. Numerical simulation on the initiation and propagation of synchronous perforating fractures in horizontal well clusters. Petrol. Explor. Dev. 266, 108412. https://doi.org/10.1016/j.engfracmech.2022.108412.
- Singh, A., Xu, S.C., Zoback, M., et al., 2019. Integrated analysis of the coupling between geomechanics and operational parameters to optimize hydraulic fracture propagation and proppant distribution. In: SPE Hydraulic Fracturing Technology Conference and Exhibition. https://doi.org/10.2118/194323-MS.
- Wang, S., Li, Z.H., Yuan, R.F., et al., 2020. A shear hardening model for cohesive element method and its application in modeling shear hydraulic fractures in fractured reservoirs. J. Nat. Gas Sci. Eng. 83, 103580. https://doi.org/10.1016/ j.jngse.2020.103580.
- Wang, Y.Z., Hou, B., Wang, D., et al., 2021. Features of fracture height propagation in cross—layer fracturing of shale oil reservoirs. Petrol. Explor. Dev. 48 (2), 1—9. https://doi.org/10.1016/S1876-3804(21)60038-1.
- Wu, K., Olson, J., Balhoff, M.T., et al., 2017. Numerical analysis for promoting uniform development of simultaneous multiple-fracture propagation in horizontal wells. SPE Prod. Oper. 32 (1), 41–50. https://doi.org/10.2118/174869-PA.
- Yang, L., Zhao, Q.M., Lyu, Q., et al., 2022. Evaluation technology and practice of continental shale oil development in China. Petrol. Explor. Dev. 49 (5), 1098–1109. https://doi.org/10.1016/S1876-3804(22)60335-5.
- Zhang, G.M., Liu, H., Zhang, J., et al., 2010. Three-dimensional finite element simulation and parametric study for horizontal well hydraulic fracture. J. Petrol. Sci. Eng. 72 (3–4), 310–317. https://doi.org/10.1016/j.petrol.2010.03.032.
- Zhang, Q.X., Hou, B., Lin, B.T., et al., 2021. Integration of discrete fracture

reconstruction and dual porosity/dual permeability models for gas production analysis in a deformable fractured shale reservoir. J. Nat. Gas Sci. Eng. 93, 104028. https://doi.org/10.1016/j.jngse.2021.104028.

Zhang, Q.X., Hou, B., Pang, H.W., et al., 2022. A comparison of shale gas fracturing based on deep and shallow shale reservoirs in the United States and China.

Comput. Model. Eng. Sci. 133 (3). https://doi.org/10.32604/cmes.2022.020831. Zhu, H.Y., Zhao, X., Guo, J.C., et al., 2015. Coupled flow-stress-damage simulation of deviated-wellbore fracturing in hard-rock. J. Nat. Gas Sci. Eng. 26, 711–724. https://doi.org/10.1016/j.jngse.2015.07.007.